Histone–Histone Interaction Mediates Chromatin Unfolding at Physiological Ionic Strength†

Martin R. Riehm‡ and Rodney E. Harrington*
Department of Biochemistry, University of Nevada, Reno, Nevada 89557
Received June 9, 1988; Revised Manuscript Received March 22, 1989

ABSTRACT: High-resolution thermal denaturation data on chicken erythrocyte chromatin are reported over 4 orders of magnitude in NaCl concentration which includes the physiological region. A novel technique using critical-point polyacrylamide sols instead of ordinary solvents effectively stabilizes chromatin against precipitation at high salt concentrations. These sols are optically transparent from 260 to 320 nm and are thermally stable over the temperature ranges studied. At Na^+ ion concentrations below 10 mM, the polyacrylamide slightly destabilizes chromatin at the nucleosome level, possibly through interactions of histones H1 and H5 with the carboxylic acid residues. At the same low salts, polyacrylamide stabilizes pure DNA against denaturation, presumably by mechanically stabilizing it against helix-distorting thermal fluctuations. In both cases, however, the polyacrylamide sols are entirely noninvasive at higher salts. Prominent low-temperature thermal transitions are observed in chromatin at and above 100 mM NaCl which evidently are associated with conformational changes in DNA. Our results are in accord with the idea that histone–histone interactions at physiological ionic strengths (~100 mM Na^+) may be comparable to histone–DNA interactions and hence may be sufficient to promote the destabilization of the DNA helix in chromatin under these conditions. The biological implications of this are discussed, and a possible model for the local decondensation of chromatin under physiological conditions is proposed.

The structure of eukaryotic chromatin has received considerable attention in recent years, and reasonable models for the supramolecular architecture of inactive chromatin from the nucleosome to the metaphase chromosomal levels have been proposed [reviewed in Newport and Forbes (1987) and Nelson et al. (1986)]. However, unfolding pathways leading to activated and active states with respect to transcription, replication, and DNA repair are not well understood [reviewed in Gross and Garrard (1988) and Weintraub (1985)]. In part, this is due to the intrinsic complexity of the problem since unfolding chromatin can evidently pass through a myriad of metastable conformational states, as with the folding and unfolding of proteins. In addition, few experimental techniques are capable of resolving these states in terms of local structure. Since both salt and temperature affect chromatin stability, it has long been assumed that combinations of these variables can lead to structural states which mimic those associated with chromatin activation.

Chromatin condenses with increasing salt in stages which evidently reflect the hierarchy of nucleosomal and fibrillar higher order structures. In vitro studies of the nucleosome conformational transition below 3 mM Na^+ suggest that flanking DNA unfolds from the core, leaving approximately one superhelical loop of DNA at the central core (Uberbacher et al., 1983; Harrington, 1982, 1981; Wu et al., 1979). Above 3 mM Na^+, chromatin is extended in the 11-nm fiber (Harrington, 1985). Between 40 and 75 mM Na^+, the nucleosomes of chromatin coil into the 30-nm fiber (Guelich et al., 1987; Widom, 1986; Harrington, 1985; Widom & Klug, 1985; Ausio et al., 1983). Above 75 mM Na^+, chromatin fibers in free solution aggregate (Ausio et al., 1983) in a manner which appears similar to chromatin packing in metaphase chromosomes (Widom, 1986).

Various histone–histone and histone–DNA interactions stabilize chromatin higher order structure and lead to cooperative folding and condensation transitions (Riehm & Harrington, 1987; Clark & Thomas, 1986; Sperling & Wachtel, 1982). At this level, histone–DNA interactions seem to be mediated largely through histone H3 and H4 N-terminal domains (Riehm & Harrington, 1987; Marion et al., 1983; Allan et al., 1982) and histone H1 and H5 C-terminal domains (Clark et al., 1988; Allan et al., 1986). Histone–histone interactions which stabilize chromatin higher order structure derive in part from N-terminal and C-terminal "head to tail" H1 and H5 interaction (Lennard & Thomas, 1985) and histones H1–H2A interaction (Boulikas et al., 1980). A variety of other histone–histone interactions may affect chromatin condensation. The ability of histone H3-H4 and histone H2A–H2B heterodimers (Sperling & Wachtel, 1982) and histone core octamers (Klug et al., 1980) to aggregate in long fibers has been documented. Structural dynamics which result from the interplay between these two types of interactions are of particular interest because chromatin, although efficient in packaging enormous lengths of DNA, is relatively transparent during biological processes requiring access to the DNA (De Bernardin et al., 1986).

Thermal denaturation studies of salt-dependent transitions in chromatin have provided high-resolution data on chromatin structural stability (Riehm & Harrington, 1987; Weischet et al., 1978). Unfortunately, past studies have been limited to very low ionic strength solvent conditions due to the large-scale aggregation and precipitation of chromatin above 75 mM NaCl noted above. In the present work, we report results of high-resolution thermal denaturation studies on chromatin over a broad range of salt concentrations including the physiological region of about 100 mM. To obtain these results, optically transparent and thermally stable high molecular weight polyacrylamide sols are used as diffusion-limiting matrices to

†Supported by U.S. Public Health Service Grant GM 33435, by Training Grant T32 CA 09563, and by Hatch Project 131 from the College of Agriculture, University of Nevada, Reno.
*Author to whom correspondence should be addressed.
‡Present address: Laboratory of Chemical Physics, NIDDK, National Institutes of Health, Bethesda, MD 20892.

0006-2960/89/0428-5787$01.50/0

control chromatin aggregation (Riehm & Harrington, 1988). Results obtained by using this method are compared at low ionic strengths with ordinary solution data on the same chromatin system, and effects due to the presence of the gel are found to be unimportant. Because the conformational state of chromatin affects its light-scattering properties, parallel measurements are taken at 320 nm and at the 260-nm optical absorption wavelength of DNA. The 320-nm data are used to correct the absorbance data for light-scattering effects and provide additional indirect information on the conformational state of the chromatin.

In the salt-dependent thermal denaturation profiles of chromatin, a remarkable change is observed at physiological ionic strength. Our results at this ionic strength suggest that histone–histone interactions leading to irreversible histone coagulation begin to dominate chromatin structural stability under these conditions. Histones H3 and H4 evidently play a central role in the aggregation process; reversibility studies of chromatin denaturation at high salt show that the susceptibility of histones toward irreversible aggregation is in the order H3 + H4 > H2a + H2b > H1 + H5 (data not shown; Riehm, 1987). This change can evidently be associated with a significant alteration in the balance of histone–DNA and histone–histone interactions which may have major biological implications.

Materials and Methods

All chemicals used were reagent grade, and all solutions were made with glass-distilled water. Acrylamide and *N*,*N*′-methylenebis(acrylamide) [bis(acrylamide)] were obtained from Bio-Rad. Acrylamide monomer stock solutions were made fresh weekly. Spectrapor dialysis tubing (grade 1, with a 6000–8000 molecular weight cutoff) was used after a 30-min soak in 0.25 mM EDTA.

Critical-point polyacrylamide sols were prepared as described previously (Riehm & Harrington, 1988).

Preparation of Chicken Erythrocyte Chromatin. Citrate-treated chicken blood was obtained from Pel-freeze Biologicals. Chicken erythrocytes and nuclei were prepared according to the method of Libertini and Small (1980). A salt-insoluble fraction of whole chicken erythrocyte chromatin was extracted from micrococcal nuclease (Worthington) digested erythrocyte nuclei according to the method of Fulmer and Bloomfield (1981) as modified for sucrose density gradient fractionation by Ausio et al. (1986).

DNA preparations were made from sucrose density gradient fractionated salt-insoluble chromatin using standard methods of proteinase K (EC 2.4.21.14, Boehringer Mannheim) digestion and phenol/chloroform/isoamyl alcohol extraction with multiple 70% (v/v) ethanol precipitation steps to remove excess phenol. All chromatin and DNA preparations were exhaustively dialyzed to 0.2 mM EDTA before use. Chromatin was routinely concentrated by using Amicon Diaflow concentrators equipped with PM30 membranes or Amicon Centricon centrifugal concentrators with the same type of membrane.

Preparation of Stock Polyacrylamide Sols. Chromatin–polyacrylamide stock sols were prepared at concentrations at or above 200 μg mL^{-1} by diluting chromatin at 4 mg mL^{-1} 1:20 with autoclaved polyacrylamide stock. These were gently mixed overnight at 4 °C using rotary inversion with a glass bead. Quantitation of the DNA in stock sols was done spectroscopically in 1-mm path-length quartz cuvettes using an extinction coefficient of 20 L g^{-1} cm^{-1}.

Five molar NaCl–polyacrylamide stock sols were prepared as described previously (Riehm & Harrington, 1988). Other, more dilute stock sols for EDTA and sodium phosphate were prepared by diluting concentrated aqueous solutions 1:10 to 25 mM Na_2EDTA and 1:5 to 100 mM NaH_2PO_4, pH 7.0, with autoclaved polyacrylamide sol. These salts were minor constituents in samples for thermal denaturation, and direct dilution facilitated quantitation of final Na^+ content.

Sample Analysis. Histone analysis was done by SDS–polyacrylamide gel electrophoresis of 0.4 N HCl extracted histone followed by high-resolution scanning of Coomassie blue R250 stained gels as outlined earlier (Riehm & Harrington, 1987).

Thermal Denaturation and Spectroscopic Measurements. Chromatin and chicken erythrocyte DNA samples for thermal denaturation in polyacrylamide were prepared and quantitated gravimetrically in silicon (Sigmacoat)-treated 25-mL side-arm flasks. Evaporation while weighing the stock sols limited accuracy to ±0.2 mg. DNA content averaged 0.73 ± 0.07 A_{260}, 1-cm path length. Allowances were made for differences in density of the concentrated NaCl stock sols. Before addition of stock NaCl, the chromatin samples were mixed on an orbital shaker with a glass bead for 30 s at 300 rpm to break up large micelles of chromatin and polyacrylamide. After addition of salt, samples were degassed under mild vacuum for 30 min. Care was taken to avoid evaporation greater than 1%.

Ultraviolet spectra were obtained routinely by using an IBM Model 9420 dual-beam UV–visible spectrophotometer. Thermal denaturation experiments at 260 and 320 nm were done on a Gilford Model 252 UV–visible spectrophotometer with a dynamic range of up to 3 optical density units (±0.001) equipped with a Model 2527 thermoprogrammer as described previously (Riehm & Harrington, 1987, 1988). Data analysis included estimation of total hyperchromicity for DNA samples. This included correcting for low- and high-temperature linear changes in absorbance according to the method outlined in Bloomfield et al. (1974) and deriving the temperature-dependent absorbance data as the fraction of nucleotide bases no longer hydrogen bonded in the DNA helix ($1 - \theta$). This approach was found suitable only for samples to which an unambiguous high-temperature base line could be assigned (generally below 70 mM Na^+ or having transitions below 78 °C). The transition melting point for these samples was estimated at 50% fraction of nucleotide bases hydrogen bonded, and the hyperchromicity was extrapolated, using low- and high-temperature base lines of the original data, back to 22 °C. Derivatives with a temperature bandwidth of 2.75 °C were obtained by a running linear least-squares computer algorithm (Riehm & Harrington, 1987). Light-scattering corrections at 260 nm for turbid chromatin suspensions were made according to the method of Riehm and Harrington (1988).

Results

Chromatin Sample Characteristics. The protein components of salt-soluble and salt-insoluble whole chicken erythrocyte chromatin were analyzed by using SDS–polyacrylamide gel electrophoresis. High-resolution scans of the stained gel showed few reproducible differences in histone content between the two chromatin fractions (data not shown), as reported previously by Ausio et al. (1986). Chromatin fragment size averaged 9500 bp as determined by agarose gel electrophoresis.

Effect of Polyacrylamide Sols on Thermal Denaturation. The ability of critical-point polyacrylamide sols to function effectively as diffusion-limiting matrices and to greatly restrict chromatin aggregation at high temperature has been previously shown (Riehm & Harrington, 1988). The rate of temperature increase used in these experiments is comparable to previous solution DNA and chromatin melting experiments (Riehm &

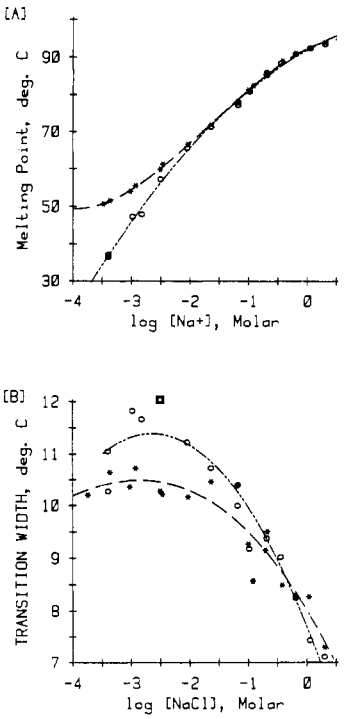

FIGURE 1: Salt-dependent melting behavior of chicken erythrocyte DNA in solution and polyacrylamide sols. (A) Transition melting points of chicken erythrocyte DNA in solution (open circles) and polyacrylamide sols (stars) plotted as a function of log NaCl concentration. The melting points below 66 mM Na^+ (log $[Na^+] = -1.18$) were obtained as discussed in the text (Materials and Methods) according to the method of Bloomfield et al. (1974). The melting points above 70 mM NaCl were taken from the temperature at maximum $d(A_{260})/dT$. (B) Salt-dependent transition mean widths for DNA in solution (open circles) and in polyacrylamide sols (stars) as a function of log NaCl concentration. Each point is the breadth of the derivative transition curve at $1/e$ of maximum height in degrees centigrade.

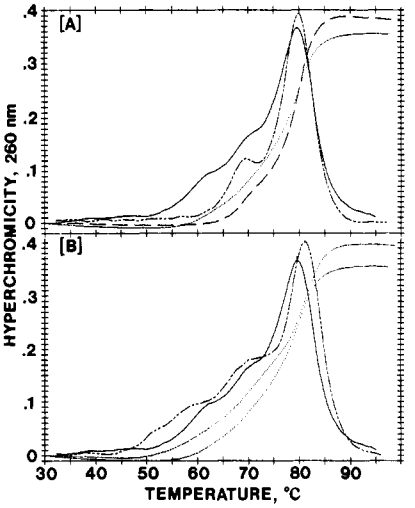

FIGURE 2: Thermal hyperchromicity curves at 260 nm for chromatin in polyacrylamide sols and in solution. (A) Salt-insoluble chromatin in polyacrylamide sols (solid derivative curve) and in solution (dashed derivative curves). Corresponding integral curves are shown normalized to derivative peak maxima. Chromatin was diluted and mixed with hydrolyzed polyacrylamide as discussed in the text (Materials and Methods). Optical density of samples was 0.7 A_{260} unit, 1-cm path length. EDTA was supplemented to 0.2 mM using concentrated aqueous stock. Parallel solution experiments were run under identical conditions. The polyacrylamide curves represent an average of three independent experiments. The solution curves represent an average of two independent experiments. (B) Salt-insoluble chromatin in polyacrylamide sols (solid derivative curve) and salt-soluble chromatin in solution (dashed derivative curves). The polyacrylamide curves are the same as in Figure (A). The curves for salt-soluble chromatin in solution are an average of two independent experiments.

Harrington, 1987) and leads to comparable reproducibility of results. Since a direct comparison is made between free solution and polyacrylamide sol denaturation profiles for chicken erythrocyte DNA (Figure 1) and chromatin (Figure 2) at low salt, we find no evidence for nonequilibrium melting in the polyacrylamide matrix.

The data of Figures 1 and 2 also address the effect of the polyacrylamide sol on the thermal denaturation profiles of both DNA and chromatin. It can be seen from Figure 1A that DNA in polyacrylamide sols melts at higher temperatures than in free solution at ionic strengths below 10 mM Na^+. Above 20 mM Na^+, DNA in the two matrices melts identically. Thus, the polyacrylamide sol appears to stabilize DNA against melting only at very low Na^+ concentrations. Figure 1B shows similar differences below 10 mM Na^+ in the mean widths or sharpness of the temperature span over which melting occurs. In free solution, the mean width for DNA is 11.3 ± 0.6 °C while in polyacrylamide sols it is reduced to 10.4 ± 0.2 °C. Again, this difference disappears above 20 mM Na^+. These results suggest that the polyacrylamide sols both stabilize and lead to an increase in melting cooperativity for DNA below 10 mM Na^+ but do not affect its melting behavior at higher salts.

In contrast, polyacrylamide sols appear to destabilize salt-insoluble chromatin at the nucleosome level at low ionic strengths. In Figure 2A, the premelt transition for chromatin in the polyacrylamide sol is larger than that of free solution. This suggests that interactions between histones H1 and H5 and the nucleosome linker DNA are reduced (Ausio et al., 1986; Cowman & Fasman, 1980) in the polyacrylamide matrix. However, from Figure 2B, it is clear that the premelt transition at low salt is larger for the salt-soluble chromatin fractions in solution than for the salt-insoluble fractions in polyacrylamide [see also Ausio et al. (1986)]. It therefore appears that the decrease in local stability induced in salt-insoluble chromatin by polyacrylamide interactions is not significant. Due to the low concentration of carboxylic acid residues estimated for these hydrolyzed polyacrylamide sols (no greater than 18 mM at a polyacrylamide concentration of 7.4 g/L; Riehm & Harrington, 1988), specific interactions of these residues with the histones at intermediate and physiological ionic strengths would be severely limited. Thus, the polyacrylamide sol may play a role in the thermal denaturation of chromatin at higher salt concentration by mechanically stabilizing the chromatin fibers in a concentrated, inert gel which may mimic the intranuclear environment in many important respects.

Salt-Dependent Thermal Denaturation of Chromatin. Figure 3 shows thermal denaturation curves as a function of salt concentration for salt-insoluble chromatin in polyacrylamide sols monitored at 260 nm (Figure 3A) and at 320 nm (Figure 3B). The absorbances at the two wavelengths are normalized to the 260-nm absorbance of the DNA used to prepare the sample, and hence the two curves are comparably scaled. The changes in light scattering with salt concentration seen in the 30 °C isotherm in Figure 3B can be associated with four distinct domains of Na^+ concentration and chromatin conformation. Below 10 mM Na^+, chromatin is extended and scatters relatively little light. From 10 to 70 mM Na^+, the gradually increasing light scattering may be associated with chromatin folding into the 30-nm fiber. Above 70 mM Na^+, the light scattering increases rapidly with salt, reaching a maximum at 200 mM Na^+. This region appears to be associated with interfiber condensation or aggregation. From about

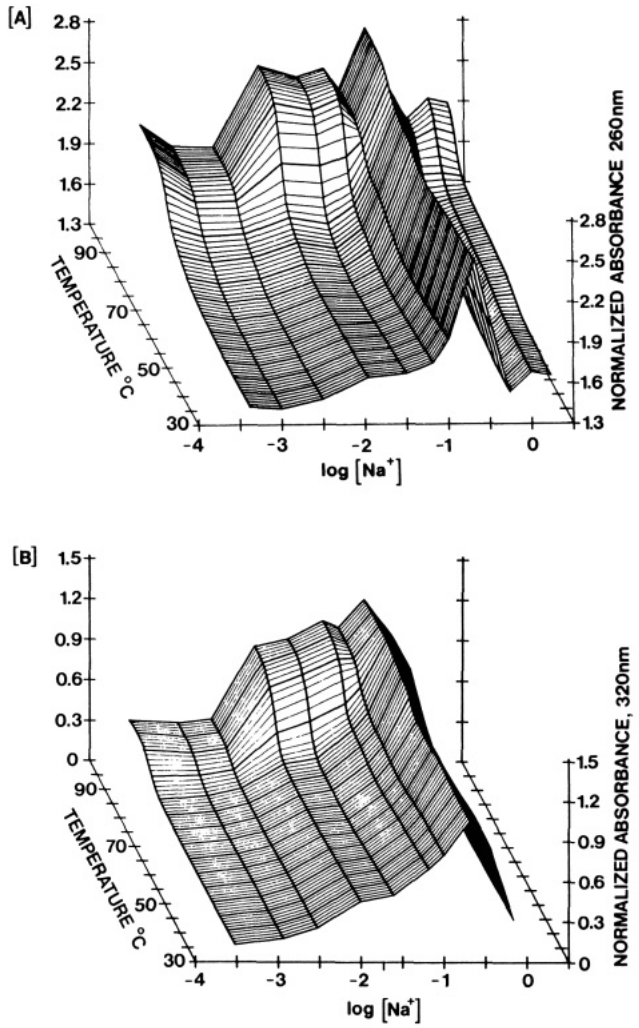

FIGURE 3: Integral thermal denaturation curves for salt-insoluble chicken erythrocyte chromatin in polyacrylamide sols as a function of salt concentration. Polyacrylamide sol concentrations were all very close to 7.3 mg mL^{-1}. DNA assays of all samples were 0.75 A_{260} unit, 1-cm path length. (A) Salt and temperature dependence of chromatin absorbance at 260 nm. The range of Na^+ concentrations shown is from 0.41 mM EDTA to 1.89 M NaCl, 5 mM NaH_2PO_4, 0.2 mM EDTA. Temperature isotherms are plotted at 1 °C intervals. (B) Same series as in (A) monitored at 320 nm. The absorbances at 260 and 320 nm are all normalized to input DNA absorbance based on gravimetric preparation of the samples with stock sols quantitated spectroscopically (see Materials and Methods). Hence, the scaling of absorbancies is identical with that in (A).

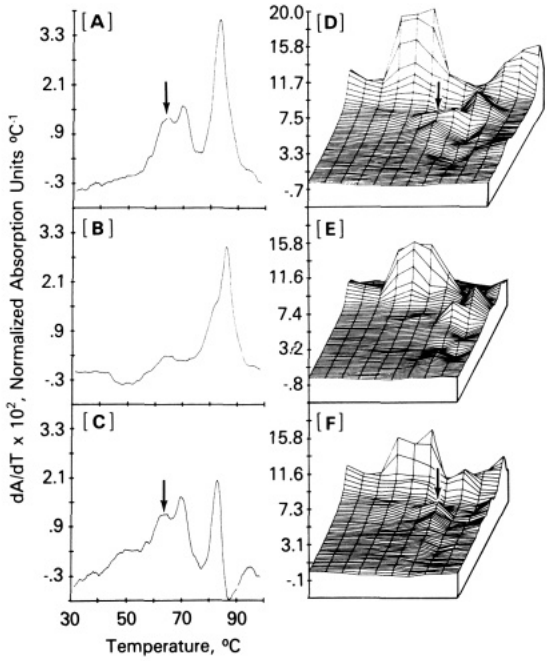

FIGURE 4: Derivative melting profiles of salt-insoluble chicken erythrocyte chromatin at 100 mM Na^+ (A–C) and from the salt concentration series plotted axonometrically (D–F) measured at 260 nm (A and D) and 320 nm (B and E) and light-scattering-corrected data measured at 260 nm (C and F). Sample preparation and other experimental conditions as in Figure 2. Derivatives were taken by using a running linear least-squares computer algorithm with a temperature bandwidth of 2.75 °C as discussed in the text (Materials and Methods). Light-scattering corrections were done according to the method of Riehm and Harrington (1988). For the axonometric plots, denaturation curves for particular salt concentrations are plotted incrementally along the x axis from lower to higher salt concentration. The view into the page is from lower to higher temperature (31 to 98.5 °C), with isotherms plotted at 1 °C intervals. The actual salt concentrations are the following (from the leftmost curve in D): 0.41 mM, 0.1 mM, 3.1 mM, 11.0 mM, 31.6 mM, 66.1 mM, 101 mM, 209 mM, 365 mM, 643 mM, 1.12 M, 1.89 M sodium. The arrows point out low-temperature transition peaks observed at 100 mM Na^+ as discussed in the text.

350 mM to 2 M Na^+, a precipitous drop in light scattering is observed. This corresponds to dissociation of histones H1 and H5, chromatin unfolding, and further dissociation of the core histones.

Some histone aggregation evidently occurs during denaturation, even below 10 mM Na^+. However, the greatest net increase in absorbance (Figure 3A) and turbidity (Figure 3B) with temperature is observed between 10 and 70 mM Na^+. This strongly suggests that in this region much histone aggregation is occurring at the same temperature at which DNA is melting within the 30-nm fiber (Riehm & Harrington, 1988). At physiological ionic strength, chromatin aggregation predominates, even at low temperature; changes in light scattering and absorbance as temperature is increased are superimposed on the high initial (30 °C) absorbance.

Our results show a clear demarcation between chromatin melting at intermediate and at higher (physiological) ionic strengths. This appears as a sharp dip at about 100 mM Na^+ in both absorbance and turbidity at the high-temperature end of the melting series in Figure 3. The phenomenon is reproducible for salt-insoluble chromatin samples with up to 2 times higher concentration of chromosomal DNA than used in this series of experiments and with salt-soluble chromatin, again at 100 mM Na^+ [data not shown; see Riehm (1987)]. The relative decrease in light scattering at the high-temperature end of the melting curve suggests that the formation of massive aggregates during denaturation at intermediate ionic strength is subdued during the melting process at 100 mM Na^+.

To help visualize the subtle transitions observed along the salt concentration series, derivatives of the melting curves were taken. Data from the melting experiments at 100 mM Na^+ are shown in Figure 4A–C, and the entire salt-dependent series is plotted axonometrically in Figure 4D–F. The data shown in Figure 4A,D are from experiments monitored at 260 nm and normalized to the absorbance of the DNA in the sample. The transitions observed in these denaturation profiles are a combination of light-scattering effects due to global changes in chromatin structure (monitored at 320 nm in Figure 4B,E), true hyperchromicity effects due to conformational changes associated with DNA melting, and anomalous light-scattering artifacts at the nucleotide transition wavelength (Riehm & Harrington, 1988).

It is instructive to group the data of Figure 4D–F into the four domains of chromatin structure discussed above. Three curves are shown for each of the low, intermediate, physio-

logical, and greater than physiological ionic strength domains. The three right-hand curves (highest salt) in Figure 4D are (left to right) 643 mM, 1.1 M, and 1.9 M Na^+, respectively. The highest salt curve in Figure 4E is 672 mM Na^+. Figure 4D,E clearly shows distinct, sharp, salt-dependent transitions at temperatures well below the main melting transitions at and above 200 M Na^+. The dips in light-scattering intensity at 50 °C begin at about 100 mM Na^+ (Figure 4B) and become more intense and cooperative at 200 and 360 mM Na^+ (Figure 4E), suggesting a relaxation or opening up of chromatin fiber aggregates. At 200 mM Na^+, the sharp increase in scattered intensity at 69 °C above these dips suggests that long-range histone–histone interactions can promote cooperative histone aggregation or "salting out" once the fibers are opened [Figure 4E; see also Figure 5 in Riehm and Harrington (1988)]. Once salting out occurs, the DNA appears to melt at the expected temperature. This is a reasonable and not unexpected observation, but it is interesting that under these conditions such salting out evidently occurs only from a chromatin fiber that is already loosened or somewhat unfolded.

To interpret the denaturation data, we use as a measure of chromatin stability the temperature at which chromatin DNA melting or conformational transitions occur relative to the expected temperature for melting transitions of histone-free DNA at the same ionic strength. As Na^+ concentration increases, two opposing trends become apparent with respect to maintaining relative chromatin stability during the melting process. In the low and intermediate ionic strength domains, the DNA is increasingly stabilized through histone–DNA interactions (Riehm & Harrington, 1987; Fulmer & Fasman, 1979; Weischet et al., 1978), possibly assisted by increasing DNA flexibility at these salt concentrations (Hagerman, 1981; Harrington, 1970). This increase in stability leads to massive, cooperative transitions at and above 75 °C, some 10–25 °C higher than observed for protein-free DNa at the same ionic strength (compare melting point transitions in Figure 1A with those found in Figure 4 at the same ionic strength). In opposition to this trend, the histones also interact and tend to form denatured aggregates as salt concentration increases [data not shown; see Riehm (1987)]. The thermal denaturation data presented here at typical physiological ionic strengths and higher imply decreased relative stability for chromatin as evidenced by transitions which occur at lower temperatures than expected for protein-free DNA. This suggests that histone–histone interactions, which lead to aggregation, may dominate under these conditions.

Figure 4C,F shows the series of melting experiments at 260 nm corrected for light scattering as determined by the parallel series monitored at 320 nm in Figure 4B,E using the methods described earlier (Riehm & Harrington, 1988). Prominent transitions are observed at 260 nm which occur at temperatures 19 °C lower than for histone-free DNA (compare the temperature for transitions at 100 mM Na^+ marked by arrows in Figure 4A,C with the transition temperature for DNA in Figure 1 at the same ionic strength). It is noteworthy also that the low-temperature transitional increase in light scattering for the 200 mM Na^+ melting experiments at 69 °C in Figure 4D [see also Figure 5 in Riehm and Harrington (1988)] is significantly reduced at 100 mM Na^+ (Figure 4B). These observations taken together suggest that histone–histone interactions at 100 mM Na^+ are approximately in balance with histone–DNA interactions. In contrast to experiments at 200 mM Na^+ where aggregated histones are able to separate from the helix and allow the DNA to melt at normal temperatures, histone–histone interactions at 100 mM Na^+ appear to promote DNA conformational transitions.

Discussion

The crossover point where histone–histone interactions begin to dominate chromatin stability appears to be very close to 100 mM Na^+. Our results clearly show that the melting behavior of chromatin is unique in several respects at this salt concentration. Most significantly, we observe the appearance of lower temperature transitions at about 63 °C in addition to the main transition at 82 °C (Figure 4A). These transitions are prominent even after light-scattering corrections (Figure 4C) and could be due either to an opening up of the chromatin aggregate, which would allow a relative increase in DNA absorbance, or to hyperchromic effects due to melting of the DNA helix. Since there is no simultaneous increase in nucleotide absorbance (260 nm) for samples at 200 mM Na^+ during the transition involving a decrease in turbidity at 53 °C [see Figure 5 in Riehm and Harrington (1988) and Riehm (1987)], and there is no decrease in turbidity (Figure 4B) coincident with the low-temperature nucleotide transitions at 100 mM Na^+ (Figure 4A), these light-scattering-corrected transitions are evidently associated with local or regional melting of DN*A*. These results suggest that the bending and supercoiling free energy of DNA packaged in eukaryotic chromatin can destabilize regions of the DNA helix if the stabilizing effects of histone–DNA interactions are effectively balanced by cooperative histone–histone interactions.

The free energy required to lower the melting transition of DNA at 100 mM Na^+ from 82 to 63 °C is approximately 430 cal (mol base pair)$^{-1}$ assuming a helix to coil enthalpic change of 8 kcal (mol base pair)$^{-1}$ (Sober, 1968). Estimates for the bending free energy of DNA wrapped around a nucleosome at 60 °C and 100 mM Na^+ range from 110 cal (mol base pair)$^{-1}$ [Record et al. (1981) using corrected temperature-dependent persistence length data from Harrington (1977)] to 200 cal (mol base pair)$^{-1}$ based on a mean DNA radius in the nucleosome of 4.55 nm (Record et al., 1981; Camerini-Otero & Felsenfeld, 1977; Landau & Lifshitz, 1958). Both the above estimates are based on a persistence length of 37.0 nm for DNA at 100 mM Na^+ (Record et al., 1981); they are increased by about 50% if this value is increased to 50.0 nm (Hagerman, 1988; Cairney & Harrington, 1982; Rizzo & Schellman, 1981). Although the differences are not large, even the most optimistic of these estimates for DNA bending free energy cannot fully account for the observed destabilization of chromatin DNA at 100 mM Na^+. To make up the difference, additional mechanisms for (regional) DNA destabilization must be examined.

We are restricted to mechanisms which involve chromatin unfolding subject to the mechanical constraints of the polyacrylamide matrix. There are two ways in which the potential energy of the coiled DNA might be increased: (1) by sharply bending the fiber, which would maintain or increase light-scattering intensity; or (2) by stretching the fiber, which would decrease the light-scattering intensity. The latter appears more probable since light scattering decreases in intensity during melting at 100 mM Na^+ relative to the intensities both above and below 100 mM Na^+ (Figure 3), since there is a minor transitional decrease in light-scattering intensity centered at 50 °C before the onset of DNA melting at this ionic strength (Figure 4B), and since the postulated micellar nature of the polyacrylamide–chromatin coacervate would likely favor longitudinal conformational changes in the chromatin fiber.

The above considerations suggest a possible model for chromatin unfolding at physiological salt conditions. We propose that the bending free energy required to package DNA

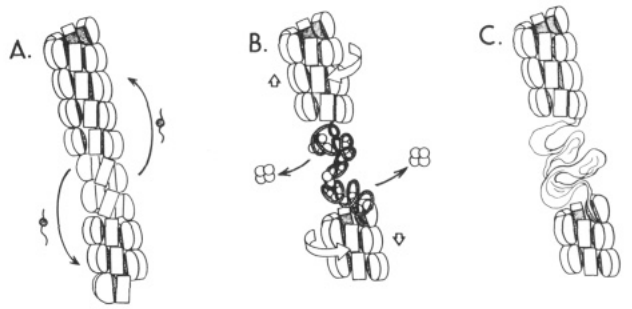

FIGURE 5: Possible model for the destabilization of the DNA helix in whole chromatin at physiological ionic strengths (about 100 mM NaCl) during thermal denaturation in polyacrylamide sol. (A) Thermal fluctuations disrupt and stretch the central portion of the 30-nm fiber, causing histone H1 to dissociate and bind to the ends of the fiber which remain intact. (B) Binding of histone H1 at the ends of the fiber results in increased packing of nucleosomes and promotes the longitudinal extension of the central H1-stripped portion. (C) The decreased radius of curvature and increased longitudinal stress of the DNA in the central portion of the fiber promote core histone dissociation and melting of the DNA helix.

in chromatin can become available to unwind or destabilize regions of the DNA helix when histone–histone and histone–DNA interactions become approximately equivalent. The available bending free energy may be supplemented by a stretching of those portions of the chromatin fiber which are mechanically constrained by the polyacrylamide matrix. Such stretching may be facilitated by histone–histone interactions. A cartoon of a possible scheme which is consistent with our observations is shown in Figure 5. At about 100 mM Na^+, the physiological saline level, histone–DNA and histone–histone interactions are approximately in balance. Regions of the 30-nm fiber are also mechanically locked in place in a concentrated gel on the surface of the chromatin–polyacrylamide micelle. Histone H1 is easily displaced at this Na^+ concentration [see especially Widom (1986) and also Thomas and Rees (1983) and Caron and Thomas (1981)]. Thermal fluctuations might then result in local stretching of the fiber and displacement of histone H1 (Figure 5A). The cooperative binding of histone H1 to intact portions of the fiber (Clark & Thomas, 1986) could induce tighter coiling of the linker DNA (Marion et al., 1985; Kaplan et al., 1984; McGhee et al., 1983a) and further promote stretching of the H1-stripped regions. As the H1-stripped portion of the fiber stretches, core histone octamers could then be displaced due to the decreased radius of curvature of the DNA and the availability of binding sites on nucleosomes in other chromatin fibers (Ausio et al., 1984; Stein, 1979; Figure 5B). This process might be further augmented by aggregation of histones H3 and H4. The resulting underwinding torsional stress on the DNA could then result in destabilization of the helix in these histone-deficient regions (Figure 5C). In the cell nucleus, such processes might be further mediated by the effects of histone acetylation, the binding of non-histone proteins, and other factors.

Although speculative, the above model may provide some insight for the regulated unwinding of chromatin and the DNA helix which also take place in a milieu of concentrated, condensed chromatin. Our results suggest a possible mechanism by which the DNA helix can be destabilized in vivo through the contractile action of chromatin mediated by histone–histone interactions. Actively transcribed genes contain nuclease-hypersensitive sites which appear to be due to torsional strain resulting in segments of non-B-form DNA [reviewed in Gross and Garrard (1988) and Weintraub (1985)]. Such destabilization of DNA may also facilitate the formation of topologically stressed looped domain complexes with specific proteins in control of transcription and site-specific transactional events.

Acknowledgments

We thank Dr. Jakob Waterborg, Dr. Don Rau, and Dr. Jim Hofrichter for many valuable discussions and suggestions.

References

Allan, J., Mitchell, T., Harborne, N., Bohm, L., & Crane-Robinson, C. (1986) *J. Mol. Biol. 187*, 591–601.

Ausio, J., & Van Holde, K. E. (1986) *Biochemistry 25*, 1421–1428.

Ausio, J., Borochov, N., Kam, Z., Reich, M., Seger, D., & Eisenberg, H. (1983) in *Structure, Dynamics, Interactions and Evolution of Biological Macromolecules* (Helene, C., Ed.) pp 89–100, D. Reidel Publishing Co., Dordrecht, The Netherlands.

Ausio, J., Seger, D., & Eisenberg, H. (1984) *J. Mol. Biol. 176*, 77–104.

Ausio, J., Sasi, R., & Fasman, G. D. (1986) *Biochemistry 25*, 1981–1988.

Bloomfield, V. A., Crothers, D. M., & Tinoco, I., Jr. (1974) *Physical Chemistry of Nucleic Acids*, p 302, Harper and Row, New York.

Boulikas, T., Wiseman, J. M., & Garrard, W. T. (1980) *Proc. Natl. Acad. Sci. U.S.A. 77*, 127–131.

Burton, D. R., Butler, M. J., Hyde, J. E., Phillips, D., Skidmore, C. J., & Walker, I. O. (1978) *Nucleic Acids Res. 5*, 3643–3663.

Cairney, K. L., & Harrington, R. E. (1982) *Biopolymers 21*, 923–934.

Camerini-Otero, R. D., & Felsenfeld, G. (1977) *Nucleic Acids Res. 4*, 1159–1181.

Caplan, A., Kimura, T., Gould, H., & Allan, J. (1987) *J. Mol. Biol. 193*, 57–70.

Caron, F., & Thomas, J. O. (1981) *J. Mol. Biol. 146*, 513–537.

Clark, D. J., & Thomas, J. O. (1986) *J. Mol. Biol. 187*, 569–580.

Clark, D. J., Hill, C. S., Martin, S. R., & Thomas, J. O. (1988) *EMBO J. 7*, 69–75.

Cowman, M. K., & Fasman, G. D. (1980) *Biochemistry 19*, 532–541.

De Bernardin, W., Koller, T., & Sogo, J. M. (1986) *J. Mol. Biol. 191*, 469–482.

Felsenfeld, G., & McGhee, J. D. (1986) *Cell (Cambridge, Mass.) 44*, 375–377.

Fulmer, A. W., & Fasman, G. D. (1979) *Biopolymers 18*, 2875–2891.

Fulmer, A. W., & Bloomfield, V. A. (1981) *Proc. Natl. Acad. Sci. U.S.A. 78*, 5968–5972.

Greulich, K. O., Wachtel, E., Ausio, J., Seger, D., & Eisenberg, H. (1987) *J. Mol. Biol. 193*, 709–721.

Gross, D. S., & Garrard, W. T. (1988) *Annu. Rev. Biochem. 57*, 159–197.

Hagerman, P. (1981) *Biopolymers 20*, 1503–1535.

Hagerman, P. (1988) *Annu. Rev. Biophys. Biophys. Chem. 17*, 265–286.

Harrington, R. E. (1970) *Biopolymers 9*, 159–193.

Harrington, R. E. (1977) *Nucleic Acids Res. 4*, 3519–3535.

Harrington, R. E. (1978) *Biopolymers 17*, 919–936.

Harrington, R. E. (1981) *Biopolymers 20*, 719–752.

Harrington, R. E. (1982) *Biochemistry 21*, 1177–1186.

Harrington, R. E. (1985) *Biochemistry 24*, 2011–2021.

Imai, B. S., Yau, P., Baldwin, J. P., Ibel, K., May, R. P., & Bradbury, E. M. (1986) *J. Biol. Chem. 261*, 8784–8792.

Kaplan, L. J., Bauer, R., Morrison, E., Langan, T. A., & Fasman, G. D. (1984) *J. Biol. Chem. 259*, 8777–8785.
Klug, A., Rhodes, D., Smith, J., Finch, J. T., & Thomas, J. O. (1980) *Nature 287*, 509–516.
Komaiko, W., & Felsenfeld, G. (1985) *Biochemistry 24*, 1186–1193.
Landau, L., & Lifshitz, E. (1958) *Statistical Physics*, pp 478–482, Pergamon Press, London.
Lennard, A. C., & Thomas, J. O. (1985) *EMBO J. 4*, 3455–3462.
Libertini, L. J., & Small, E. W. (1980) *Nucleic Acids Res. 8*, 3517–3534.
Marion, C., Pallotta, L., & Roux, B. (1982) *Biochem. Biophys. Res. Commun. 108*, 1551–1558.
Marion, C., Hesse-Bezot, C., Bezot, P., Marion, M. J., Roux, B., & Bernengo, J. C. (1985) *Biophys. Chem. 22*, 53–64.
McGhee, J. D., Nickol, J. M., Felsenfeld, G., & Rau, D. C. (1983a) *Cell (Cambridge, Mass.) 33*, 831–841.
McGhee, J. D., Nickol, J. M., Felsenfeld, G., & Rau, D. C. (1983b) *Nucleic Acids Res. 11*, 4065–4075.
McMurray, C. T., & van Holde, K. E. (1986) *Proc. Natl. Acad. Sci. U.S.A. 83*, 3472–3476.
Morgan, J. E., & Matthews, H. R. (1987) *Fed. Proc., Fed. Am. Soc. Exp. Biol. 46*, 2171.
Nelson, W. G., Pienta, K. J., Barrack, E. R., & Coffey, D. S. (1986) *Annu. Rev. Biophys. Biophys. Chem. 15*, 457–475.
Newport, J. W., & Forbes, D. J. (1987) *Annu. Rev. Biochem. 56*, 535–565.
Oohara, I., & Wada, A. (1987) *J. Mol. Biol. 196*, 399–411.
Paponov, V. D., Gromov, P. S., Sokolov, N. A., Spitkovsky, D. M., & Tseitlin, P. I. (1980) *Eur. J. Biochem. 107*, 113–122.
Riehm, M. R. (1987) Dissertation, University of Nevada, Reno.
Riehm, M. R., & Harrington, R. E. (1987) *Biochemistry 26*, 2878–2886.
Riehm, M. R., & Harrington, R. E. (1988) *Anal. Biochem. 172*, 296–303.
Rizzo, V., & Schellman, J. A. (1981) *Biopolymers 20*, 2143–2163.
Rocha, E., Davie, J. R., Van Holde, K. E., & Weintraub, H. (1984) *J. Biol. Chem. 259*, 8558–8563.
Russev, G., Vassilev, L., & Tsanev, R. (1980) *Mol. Biol. Rep. 6*, 45–49.
Seligy, V. L., & Poon, N. H. (1978) *Nucleic Acids Res. 5*, 2233–2252.
Sen, D., & Crothers, D. M. (1986) *Biochemistry 25*, 1495–1503.
Simon, R. H., Camerini-Otero, R. D., & Felsenfeld, G. (1978) *Nucleic Acids Res. 5*, 4805–4818.
Sober, H. (1968) *The Handbook of Biochemistry*, Chemical Rubber Co., Cleveland, OH.
Sperling, R., & Wachtel, E. J. (1981) *Adv. Protein Chem. 34*, 1–60.
Stein, A. (1979) *J. Mol. Biol. 130*, 103–134.
Thomas, J. O., & Rees, C. (1983) *Eur. J. Biochem. 134*, 109–115.
Tsuboi, M., Matsuo, K., & Ts'o, P. O. P. (1966) *J. Mol. Biol. 15*, 256–267.
Uberbacher, E. C., Ramakrishnan, V., Olins, D. E., & Bunick, G. J. (1983) *Biochemistry 22*, 4916–4923.
Volkenstein, M. V. (1963) *Configurational Statistics of Polymeric Chains*, pp 373–376, Interscience, New York.
Wada, A., Yabuki, S., & Husimi, Y. (1980) *CRC Crit. Rev. Biochem. 9*, 87–144.
Weintraub, H. (1984) *Cell (Cambridge, Mass.) 38*, 17–27.
Weintraub, H. (1985) *Cell (Cambridge, Mass.) 42*, 705–711.
Weisbrod, S. (1982) *Nature (London) 297*, 289–295.
Weischet, W. O., Tatchell, K., Van Holde, K. E., & Klump, H. (1978) *Nucleic Acids Res. 5*, 139–160.
Widom, J. (1986) *J. Mol. Biol. 190*, 411–424.
Widom, J., & Klug, A. (1985) *Cell (Cambridge, Mass.) 43*, 207–213.
Wilhelm, M. L., & Wilhelm, F. X. (1980) *Biochemistry 19*, 4327–4331.
Wu, H. M., Dattagupta, N., Hogan, M., & Crothers, D. M. (1979) *Biochemistry 18*, 3960–3965.
Zama, M., Bryan, P. N., Harrington, R. E., Olins, A. L., & Olins, D. E. (1977) *Cold Spring Harbor Symp. Quant. Biol. 42*, 31–42.